Desalination and Water Treatment
www.deswater.com
doi: 10.5004/dwt.2023.29150

281 (2023) 287–295
January

Photocatalytic properties of bismuth oxyiodide nanomaterials with different morphologies

Ji-wei Zhao[a], Zhi-qiang Wei[a,b], Shang-pan Huang[a], Ling Li[a], Jin-huan Ma[a,*]

[a]*School of Science, Lanzhou University of Technology, Lanzhou 730050, China, email: qianweizuo@163.com (J.-h. Ma)*
[b]*State Key Laboratory of Advanced Processing and Recycling of Non-Ferrous Metals, Lanzhou University of Technology, Lanzhou 730050, China*

Received 24 June 2022; Accepted 25 November 2022

ABSTRACT

The morphology of bismuth oxyiodide (BiOI) was regulated by co-precipitation method by changing the solvent dosage and pH value. X-ray diffraction, scanning electron microscopy, surface area and pore structure analyzer, high-resolution transmission electron microscopy, UV-Vis diffuse reflection spectrum (UV-Vis DRS) were used to characterize the phase structure, morphology, specific surface area and pore structure, microstructure, optical properties and band structure of the samples. In addition, the effects of morphology and amount of photocatalyst on the photocatalytic performance of BiOI were evaluated by degradation of Rhodamine B (RhB). The experimental results demonstrated that the morphology of BiOI nanopowders (flower-like, microspherical and layered) can be adjusted by changing the solvent dosage and pH value. The flower-like BiOI prepared by this method maintains a single-phase tetragonal structure with a small crystallite size and good crystallization. Flower-like structure BiOI exhibits excellent visible light absorption ability and the narrowest bandgap. Microspherical BiOI displays the best photocatalytic activity for RhB degradation. In addition, $^{\bullet}OH$, $^{\bullet}O_2^-$ and h^+ all played a certain role in the photocatalytic degradation process. And the possible photocatalytic activity mechanism was also proposed.

Keywords: Bismuth oxyiodide; Morphology; Microstructure; Photocatalytic activity

1. Introduction

Since the industrial revolution, with the growth of the world's population and the rapid development of social economy, human beings are facing more and more serious water environment pollution, which seriously threatens the ecological environment and human health [1–4]. In recent years, with the rapid development of modern industry and agriculture, a variety of environmental problems have arisen. In particular, dyestuff wastewater discharged from textile, printing and dyeing industries has attracted extensive attention due to its deep chroma and high organic content. [5,6]. At present, people have developed chemical oxidation, adsorption, flocculation precipitation, biodegradation, ozone oxidation, photocatalytic treatment methods and so on [7–9].

Semiconductor photocatalysis is a kind of degradation method with mild reaction conditions, low cost and high efficiency [10–13]. The photogenerated charge carriers can be transferred to the material surface and exhibit unique redox properties [14,15]. Therefore, it is considered to be a very effective technique for the treatment of pollutants in water. Bismuth oxyiodide (BiOI) is a P-type narrow bandgap (1.8 eV) V–IV–VII semiconductor with a layered structure consisting of halogen I atoms inserted into $[Bi_2O_2]^{2+}$ layer with the alternate combination of Van der Waals forces along the Z-axis [16–20]. Nowadays, BiOI has

* Corresponding author.

been widely used as a semiconductor photocatalyst for the treatment of pollutants due to its narrow bandgap, wide visible light absorption band and high separation rate of photogenerated carriers [21–23]. However, due to the small photocurrent response and high recombination rate of photogenerated electron–hole pairs, the practical application of BiOI is limited [24]. Therefore, to overcome the above defects, a series of strategies have been developed to improve the activity of semiconductor photocatalysts, including metal doping, defect modification, morphology control, dye sensitization, precious metal deposition, and heterostructure construction [25,26].

The photocatalytic properties of semiconductor photocatalysts are not only affected by physical properties (band structure, crystal structure, morphology, particle size and specific surface area) but also affected by external factors, such as temperature, solution pH value, photocatalyst amount, pollutant concentration, light source and illumination time [27–31]. Among them, the microstructure and grain size are the key factors affecting the photocatalytic performance of semiconductor photocatalysts [32]. Unfortunately, as far as we know, there are few studies on the effect of morphology control and the amount of photocatalyst on the photocatalytic performance of BiOI nanomaterials. Therefore, the main purpose of this study is to study the morphology regulation and photocatalytic performance of BiOI nanomaterials which prepared by the co-precipitation method.

In this work, the co-precipitation method was used to regulate the morphology of by changing the solvent dosage and pH value. BiOI photocatalysts with three-dimensional flower-like shape, microsphere and two-dimensional sheet were prepared by changing the solvent dosage and pH value. In addition, the influence of morphology and amount of photocatalyst on the photocatalytic performance of aqueous solution under simulated sunlight was proposed, and the active species were detected. The relationship between the morphology, crystal structure, photoresponse ability and photocatalytic performance of BiOI was studied in depth. At the same time, the possible enhanced visible photocatalytic activity mechanism was also proposed.

2. Experimental

2.1. Synthesis of BiOI nanopowders

BiOI nanopowders with different morphologies were fabricated by the co-precipitation method. The raw materials used in this experiment are analytical grade which does not to be further purified. The typical synthesis process of BiOI nanopowders is as follows: according to the chemical formula BiOI and the molar ratio of Bi^{3+}:I^- is 1:1, weighed stoichiometric amounts of $Bi(NO_3)_3{\cdot}5H_2O$ and KI used as precursors, $Bi(NO_3)_3{\cdot}5H_2O$ were dissolved in 50 mL solvent (as Table 1) by continuous stirring to obtain a mixed metal salt solution, and then a certain amount of KI was dissolved in 50 mL deionized water by constant magnetic stirring to form a uniform solution. Subsequently, KI solution was slowly dropped into $Bi(NO_3)_3{\cdot}5H_2O$ solution, and the resulting mixture was ultrasonic treatment for 60 min. After the pH value of above-mixed solution was adjusted to a certain value by dropping NaOH solution with magnetic stirring for 60 min.

Table 1
Preparation parameters of BiOI samples with different morphologies

Sample	Solvent	pH	Morphology
BiOI-1	Anhydrous ethanol, water	7	Flower
BiOI-2	Ethylene glycol, water	7	Microsphere
BiOI-3	Anhydrous ethanol, water	3	Sheet

Then, the mixed solution was transferred to a drying oven and treated at 80°C for 4 h. After the reaction, cooled to room temperature naturally, the obtained precipitates were washed alternately with deionized water and anhydrous ethanol several times, respectively. Finally, the sediment was dried under vacuum at 60°C for 8 h to obtain BiOI photocatalysts. Different morphologies of BiOI photocatalysts were obtained with similar methods by changing the solvent dosage and pH value, which were assigned as BiOI-1, BiOI-2 and BiOI-3, respectively.

The photocatalytic activity was measured by simulating the degradation of Rhodamine B by sunlight. A xenon lamp is used to simulate sunlight during photocatalytic degradation. Photocatalytic degradation experiment used Rhodamine B (RhB) 100 mL with an initial concentration of 5 mg/L and photocatalyst 0.01 g. Before xenon lamp irradiation, in order to achieve the adsorption–desorption balance of RhB on the surface of BiOI nanomaterials, a dark treatment operation is required, that is, the suspension is stirred for 0.5 h under dark conditions. A small amount of the solution was removed every 15 min to determine the concentration of RhB. The absorbance of the solution was measured using a visible spectrophotometer (λ = 554 nm). P-benzoquinone (1 mmol/L), isopropanol (5 mL) and methanol (5 mL) were used as the traps of $^{\bullet}O_2^-$, $^{\bullet}OH$ and h^+, respectively.

2.2. Characterization techniques

The phase structure of the as-prepared samples was analyzed by X-ray diffractometer (Rigaku, Japan, D/MAX-2400) with monochromatized Cu-Kα source (λ = 0.15406 nm). The morphology and microstructure of the products were observed by scanning electron microscopy (SEM, JEOL JSM-6701 F) and high-resolution transmission electron microscopy (HRTEM, JEM-2010). The specific surface area and pore-size distribution were calculated from nitrogen adsorption–desorption isotherms using an apparatus (Micromeritics ASAP 2020). The bandgap energy of the catalysts was measured by an ultraviolet-visible (UV-Vis) spectrophotometer (PERSEE TU-1901).

Mott–Schottky (M-S) curves of samples were measured by an electrochemical workstation in a typical three-electrode system (CorrTest, CS350). The photocatalytic degradation of RhB by xenon lamp irradiation at room temperature was evaluated by VS-GCH-XE-300 photochemical reaction apparatus, and the absorbance of the solution was measured by Shimadzu UV-1208 spectrophotometer.

Table 2
Interplanar spacing, lattice constant, crystallite size and FWHM of *BiOI* samples

Sample	2θ (°)	d_{hkl} (Å)	FWHM (°)	*D* (nm)	*a* = *b* = *c* (nm)
BiOI-1	30.01	2.98	0.49	16.56	0.808
BiOI-2	29.27	3.05	0.87	9.35	0.810
BiOI-3	29.93	2.98	0.51	15.94	0.809

3. Results and discussion

3.1. Structural characterization

Fig. 1 displays the X-ray diffraction (XRD) patterns of BiOI photocatalysts with three different morphologies. It is obvious that all samples show similar characteristic peaks at 2θ = 24.3°, 29.7°, 31.7°, 37.1°, 39.4°, 45.5°, 51.5° and 55.3°, which matched well with tetragonal BiOI (JCPDS 73-2062) and corresponding to (011), (012), (110), (013), (004), (020), (114) and (122) crystal planes, respectively. The most intense diffraction peak (012) indicates that BiOI selectively grows along the (012) crystal planes. In addition, no excess diffraction peaks are observed within the detection limit of XRD, which proves that pure BiOI with single phase was successfully prepared. Furthermore, the diffraction peak of microspherical BiOI widened at the full width at half maximum value (FWHM), indicating that the crystallinity of microspherical BiOI is inferior to layered and flower-like BiOI. In Table 2, according to Scherrer's formula: $D = K\lambda/\beta\cos\theta$, where K = 0.89, λ = 0.15406 nm, D, β and θ represents the crystallite size, full width at half maximum (FWHM) and diffraction angle [33]. The crystallite size of the product was estimated based on the most intense diffraction peak (012), and the XRD results of the samples are summarized in Fig. 1.

It can be seen that the crystallite size of microspherical BiOI-2 is the smallest synthesis with ethylene glycol and water as solvent at pH = 7, while the crystallite size of flower-like BiOI-1 is the largest synthesis with anhydrous ethanol and water as solvent at pH = 7. These results indicate that the preparation parameters (solution type and pH value) have a regulating effect on grain size, which may be caused by uneven stress or strain during grain growth.

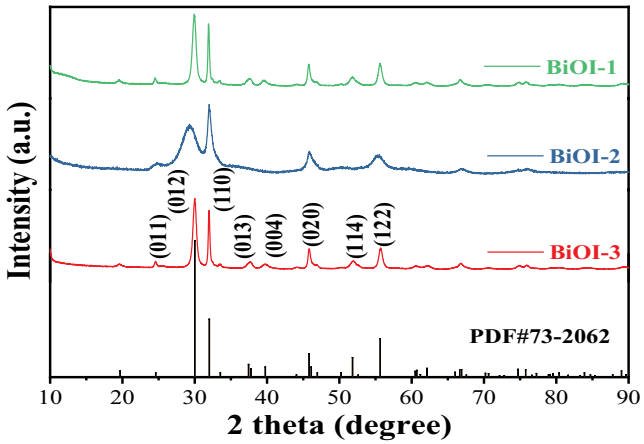

Fig. 1. XRD patterns of flower-like, microspherical and layered *BiOI*.

3.2. Morphological studies SEM analysis

Fig. 2 shows typical SEM images of BiOI samples with three different morphologies prepared under different experimental conditions. As shown in Fig. 2a, BiOI-1 samples exhibit three-dimensional flower-like structure formed by overlapping of many nanosheets, and the average diameter about 1 μm. As shown in Fig. 2b, the morphology of BiOI-2 samples is mainly three-dimensional loose porous microsphere architecture with average diameter of about 500 nm, the high surface energy and large specific surface area of the microspheres lead to light agglomeration, which can improve the adsorption capacity of photocatalyst. Therefore, the three-dimensional flower-like structure plays a positive role in improving the photocatalytic activity of BiOI nanomaterials. The SEM images of BiOI-3 samples possess two-dimensional sheet morphology with smooth surface, clear edges and thickness about 50 nm as shown in Fig. 2c. From the above analysis, it can be seen that the solution type and pH value have a significant impact on the morphology of BiOI samples prepared by the co-precipitation method, and the morphology could be effectively regulated by adjusting preparation parameters (solution type and pH value) of the reaction system.

The microstructure of flower-like BiOI was further analyzed by HRTEM, as shown in Fig. 3a and b, the three-dimensional flower-like structure composed of thin slices could be clearly observed. Fig. 3c presents the locally enlarged HRTEM image of BiOI-1 samples, where the neatly aligned lattice fringes c can be clearly observed. The measured crystal plane spacing is about 0.3016 nm, corresponding to the (012) crystal plane of tetragonal BiOI, indicating that BiOI preferentially grew along the (012) crystal plane, which is consistent with XRD results. Fig. 3d displays the selected area electron diffraction (SAED) diagram of flower-like BiOI, which consists of a series of concentric rings with different radius due to the polycrystalline structure of the sample. These diffraction rings correspond to the crystal plane (110), (012), (013) and (020) crystal plane of tetragonal BiOI from inside to outside, respectively. The SAED and HRTEM results further indicate that BiOI samples possess a tetragonal structure, which is consistent with XRD analysis results.

The co-precipitation preparation process needs to be carried out in specific reaction solvents, different solvents have different viscosity and different ion diffusion rates, thus affecting the growth of nanoparticles. BiOX is a layered structure formed by inserting X into the $[Bi_2O_2]^{2+}$ layer. The higher the solvent viscosity, the lower the ion diffusion rate and the thinner the nanosheet. Appropriate solvent can also induce the self-assembly of two-dimensional

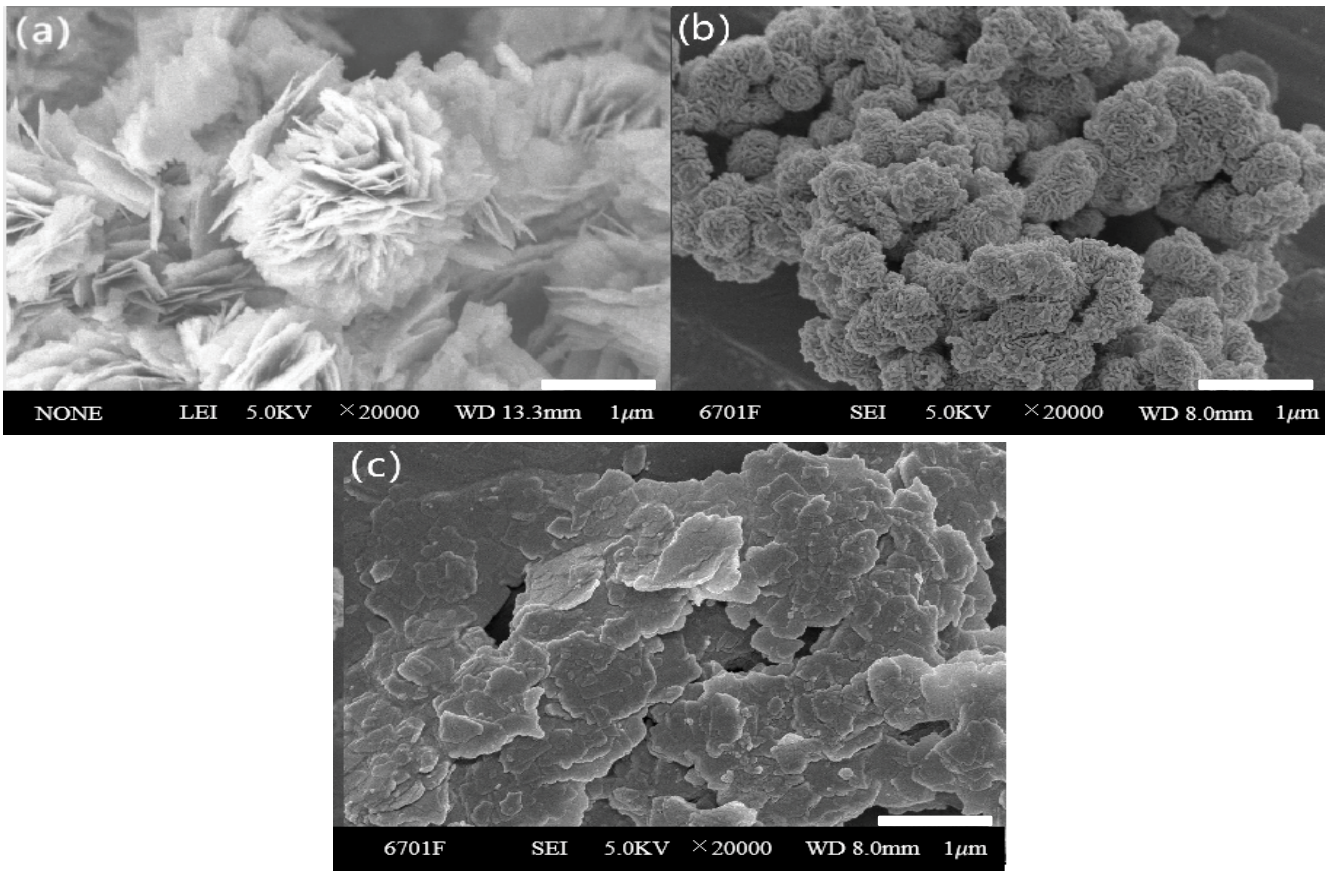

Fig. 2. SEM images of flower-like, microspherical and layered *BiOI*.

layered BiOX nanosheets into three-dimensional structures, increasing the specific surface area. In addition, the increase of H^+ concentration in the solution will slow down the rate of nucleation and growth for BiOI, and also affect the thickness of BiOI nanosheets: When the pH value decreases, the nanosheets will become thinner. The morphology analysis results of three-dimensional flower-like BiOI and two-dimensional layered BiOI showed that pH value had a significant effect on the morphology of the materials, and the morphology could be effectively regulated by adjusting the solvent dosage and pH value. Thin nanosheets facilitate the diffusion of electrons to the material surface, thus facilitating the separation of photogenerated charge carriers.

4. Optical performance analysis

UV-Vis absorption spectra of the flower-like shape, microspherical architecture and layered BiOI samples were tested to study the photoresponse ability and the bandgap, respectively, as shown in Fig. 4a. All samples show obvious absorption bands in the range of 250–500 nm, which indicates that BiOI nanopowders have better visible-range absorption features and strong light response-ability in the visible light region. The absorption edge of flower-like BiOI-1 appears at 580 nm, compared with microspherical BiOI-2 and layered structure BiOI-3. Fig. 4b shows the first derivative curves of the samples from the UV-Vis spectrum. The bandgap of the photocatalyst can be obtained according to $E_g = 1{,}240/\lambda$ (E_g and λ represent the bandgap and absorption wavelength of the semiconductor respectively) [34]. The bandgap of flower-like, microspherical and layered BiOI are 2.07, 2.33 and 2.35 eV, respectively, and flower-like BiOI exhibits the smallest bandgap.

5. Specific surface area and pore structure analysis

Fig. 5 shows the nitrogen adsorption–desorption isotherms and pore-size distribution (inset of Fig. 5) of BiOI with different morphologies, the nitrogen adsorption–desorption isotherms of flower-like, microspherical and layered BiOI samples can be classified as type IV of H3 hysteresis loop with obvious mesoporous structure characteristics [23]. The Brunauer–Emmett–Teller (BET) specific surface area for BiOI-1, BiOI-2 and BiOI-3 are 177, 190 and 157 m^2/g, respectively. Compared with BiOI-1 and BiOI-3, the specific surface area of microspherical BiOI-2 is significantly higher than that of flower-like and layered BiOI samples. In addition, the Barrett–Joyner–Halenda (BJH) pore-size distribution plot for BiOI-1, BiOI-2 and BiOI-3 samples as shown inset of Fig. 5, indicating the pore diameter mainly distributed in the typical mesoporous region within the range of 2–10 nm. The specific surface area and suitable mesoporous size can provide more active sites for

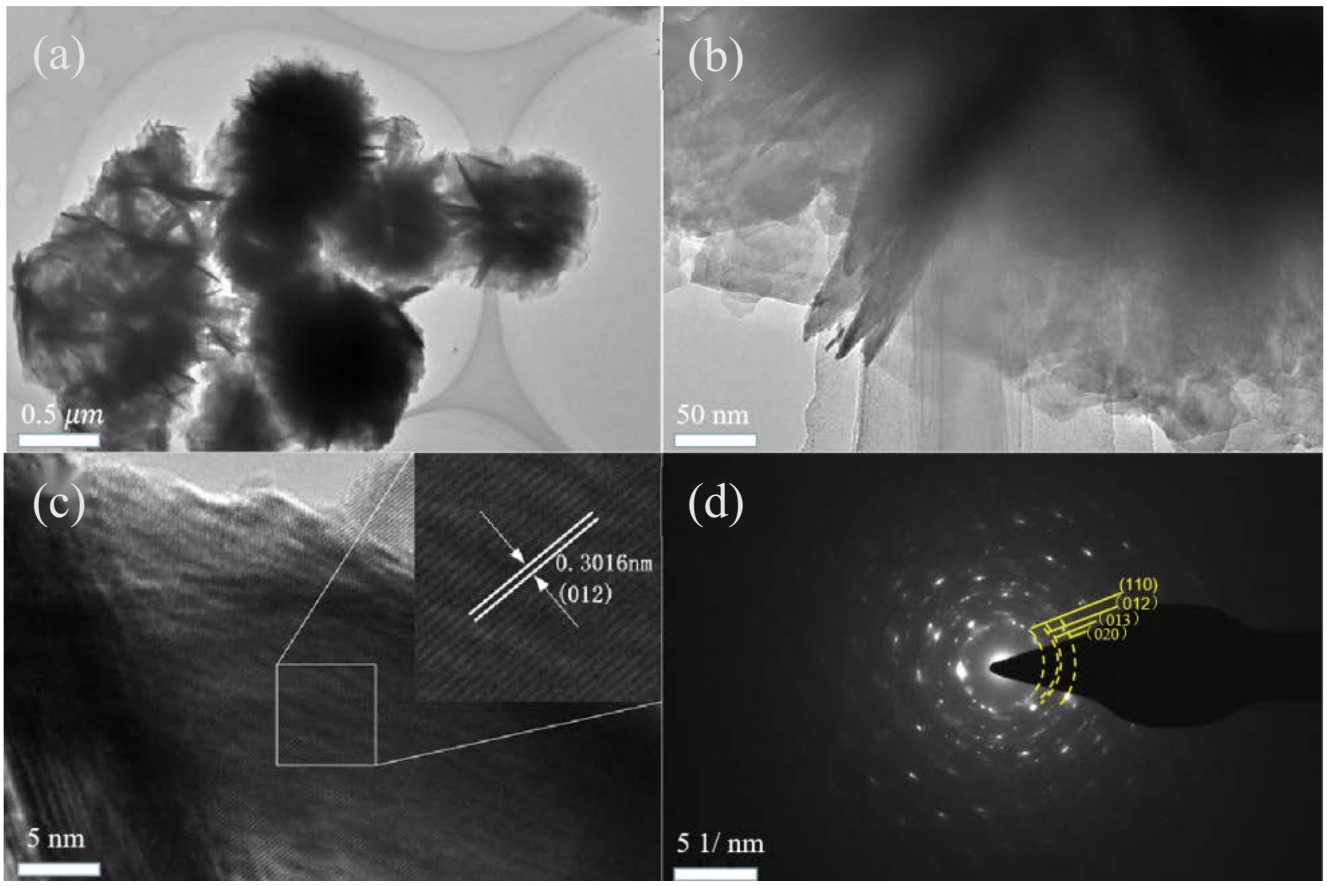

Fig. 3. (a–c) HRTEM and (d) SAED of flower-like *BiOI*.

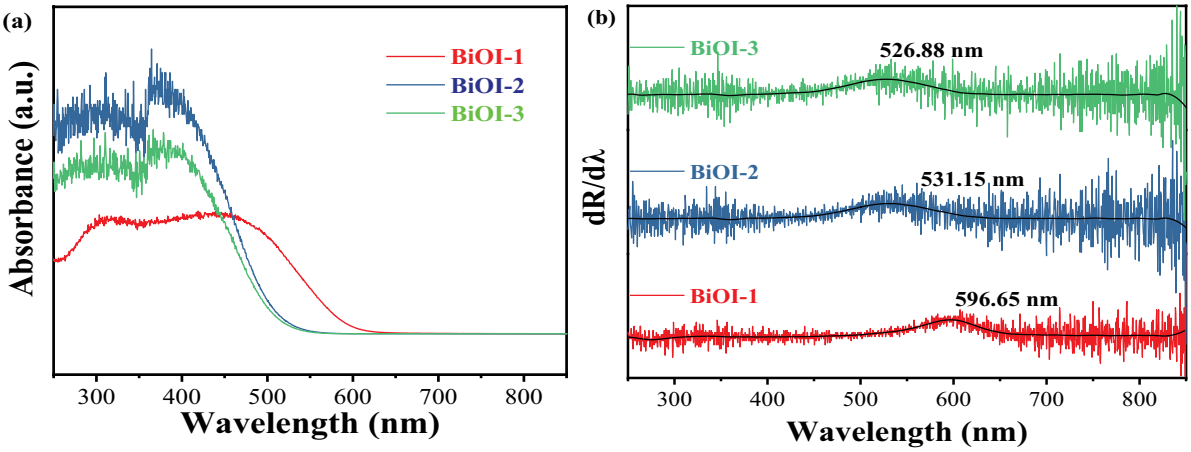

Fig. 4. (a) UV-Vis absorption spectrum and (b) first derivative curves of *BiOI* samples.

the photocatalyst, improve the separation and transport efficiency of photogenerated carriers, and improve the degradation ability of the semiconductor photocatalyst.

6. Photoelectric chemical performance analysis

Fig. 6 shows the Mott–Schottky curve for flower-like BiOI-1 samples obtained at 3,000 and 5,000 Hz. The slope in the linear region of the Mott–Schottky curve is negative indicates that BiOI is P-type semiconductor. The linear part intersected with the horizontal axis, and the horizontal axis intercept is the flat band potential E_{FB} is 0.82 V vs SCE. The valence band potential (E_{VB}) for a P-type semiconductors can be approximately equal to $E_{FB.}$ According to the formula: V(NHE) = V(SCE) + 0.059pH + 0.242 (pH = 7), the potential of the standard calomel electrode (SCE) can be

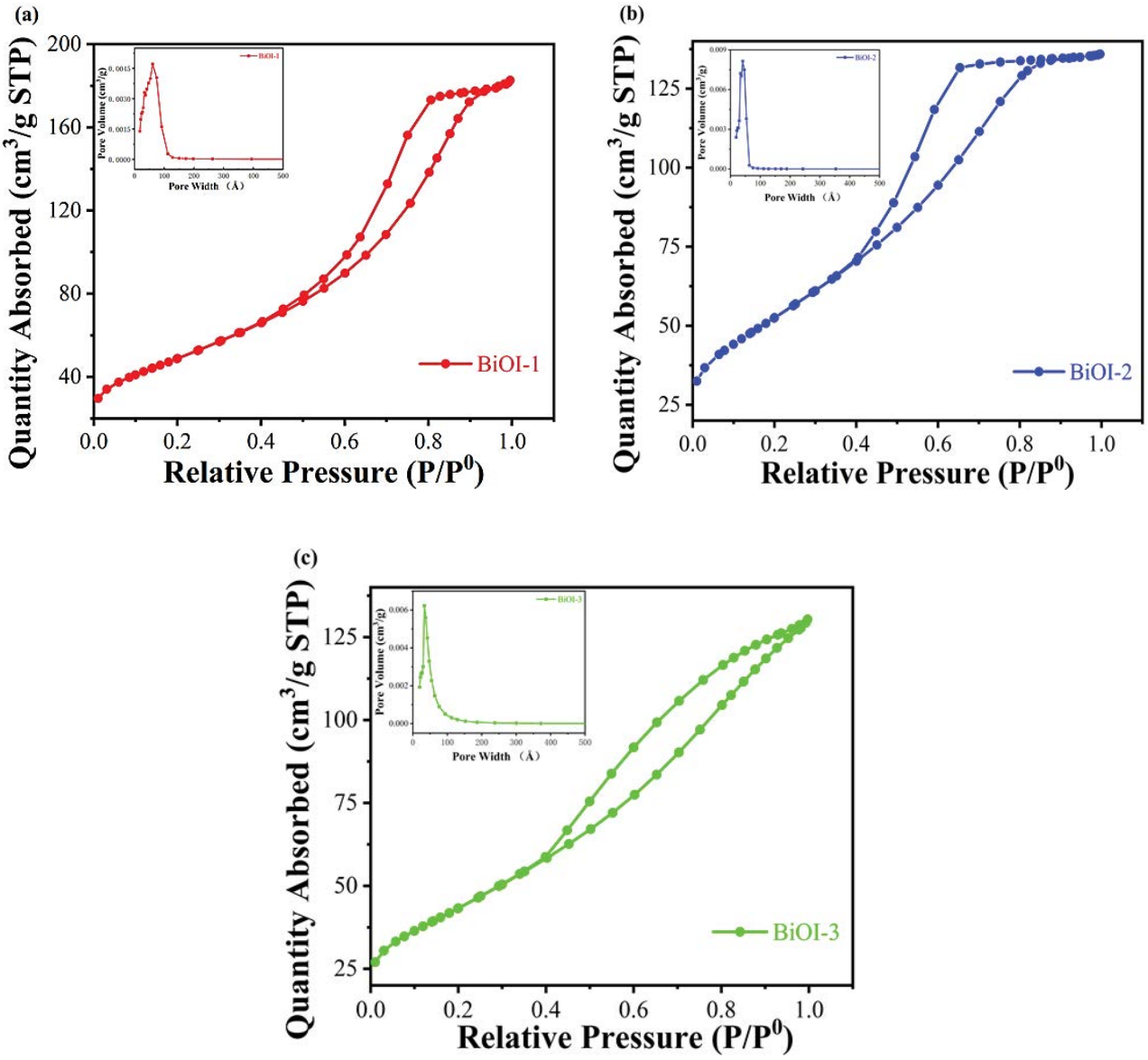

Fig. 5. Nitrogen adsorption–desorption isotherms and the pore-size distribution curve of *BiOI* samples (a) flower-like *BiOI*, (b) microspherical *BiOI* and (c) layered *BiOI*.

converted to the potential of the standard hydrogen electrode (NHE) [22]. Therefore, the corresponding E_{CB} and E_{VB} for BiOI are –0.46 and +1.47 V vs NHE, respectively.

7. Analysis of photocatalytic performance

The photocatalytic efficiency of BiOI photocatalysts was evaluated by the degradation of RhB under 200 W xenon lamp irradiation. Fig. 7a shows photocatalytic degradation curves for BiOI photocatalysts. Before each irradiation reaction, the above suspension was firstly dispersed by stirring for 30 min in dark to establish an adsorption–desorption equilibrium. Compared with BiOI-1 and BiOI-3, microspherical BiOI-2 exhibited better adsorption performance than flower-like and layered BiOI due to its larger specific surface area. The photocatalytic degradation rate for microspherical BiOI reached 92% at 90 min. In contrast, the photocatalytic degradation rate for BiOI-1 and BiOI-3 is 64.6% and 28.2% within 90 min.

Fig. 7b displays the corresponding first-order kinetics curve. It is obviously that the kinetics curves of all samples exhibit linear relationship, indicating that the photocatalytic degradation of RhB exhibit first-order kinetics characteristics: $\ln(C_0/C_t) = k_{app}t$ where C_0 and C_t, respectively the initial and residual concentrations of dye at t min after the reaction, and k_{app} is the rate constant of first-order kinetic reaction [35]. The rate constants of flower-like, microspherical and layered BiOI photocatalysts are 0.00842, 0.02403

and 0.00575 min^{-1}, respectively. And microspherical BiOI possess the highest rate constant, which is 1.5 and 8.0 times flower-like and layered BiOI, respectively.

The synergistic interaction between crystallinity, morphology and particle size of nanomaterials affects the photocatalytic performance of BiOI materials. Among three different morphologies of BiOI, microspherical BiOI show the best photocatalytic degradation efficiency, because the smaller the particle size of semiconductor material, the easier the photogenerated charge will migrate to the surface of the material. In addition, the three-dimensional structure has large specific surface area, more active sites and strong adsorption capacity, which can also make the light reflect multiple times inside the catalyst and improve the light absorption capacity. The three-dimensional flower-like BiOI has better photocatalytic activity than two-dimensional layered BiOI owing to its larger specific surface area and excellent light response ability. The synergistic effect among crystallinity, morphology and particle size of nanomaterials affects the photocatalytic performance of BiOI materials.

The amount of photocatalyst was also an important external factor affecting the degradation efficiency. The photocatalytic degradation of flower-like BiOI was carried out by the degradation of RhB under 200 W xenon lamp irradiation with 0.01, 0.03 and 0.05 g, respectively. It can be seen from Fig. 8 that the adsorption capacity of organic pollutants increases with the increase of the amount of photocatalyst. In addition, the photocatalytic degradation rate first increased rapidly with the increase of the amount of photocatalyst. However, with the prolongation of illumination time, the reaction rate gradually slowed down. This is because the more catalysts at the beginning, the more catalysts adsorbed on the dyed surface and the faster the reaction rate. However, with the progress of photocatalytic reaction, when the amount of photocatalyst is too much, the samples will cover each other, affecting the transmission and absorption of the incident light, thus further affecting the photocatalytic efficiency.

In order to investigate the reaction mechanism and determine the main active species in the process of

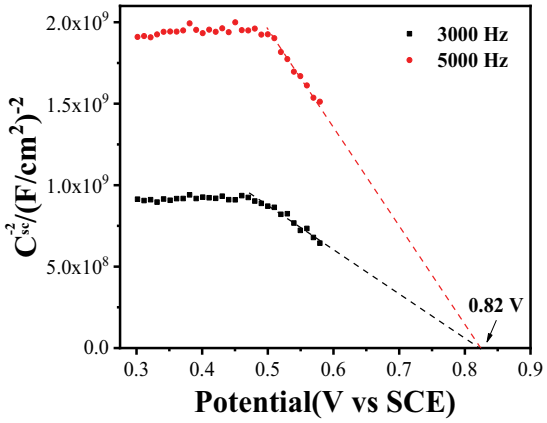

Fig. 6. M-S curve of flower-like *BiOI* samples.

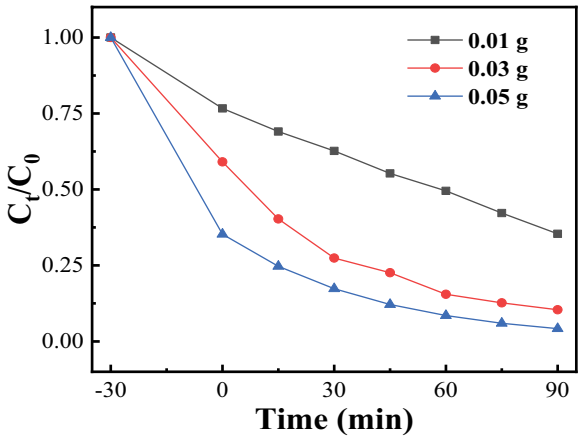

Fig. 8. Photocatalytic degradation of RhB organic pollutants by 0.01, 0.03 and 0.05 g flower-like *BiOI*.

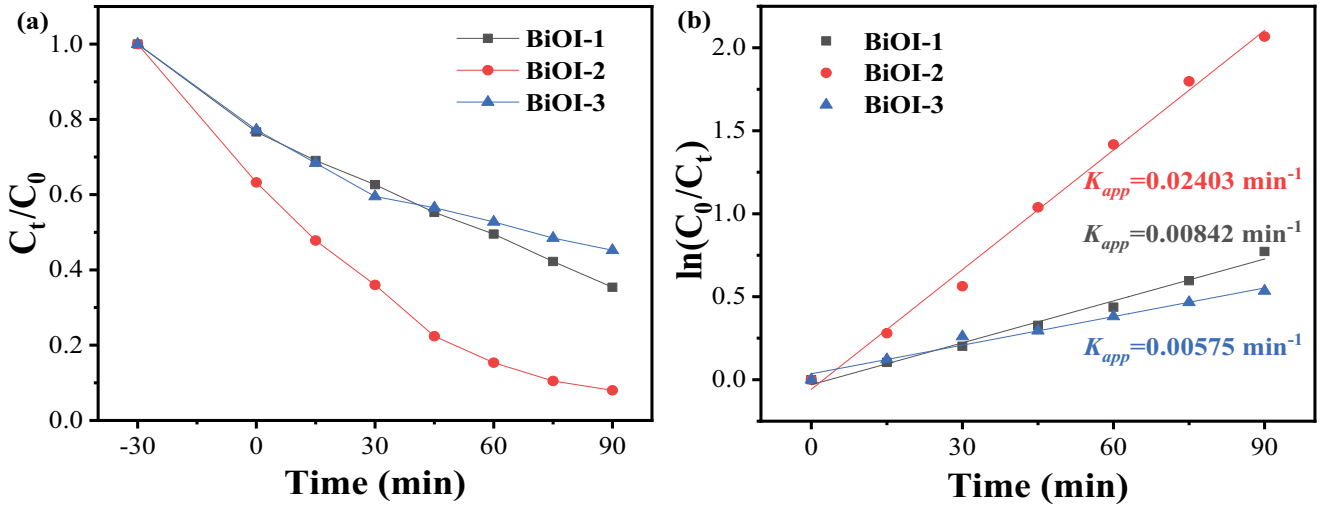

Fig. 7. (a) Photocatalytic degradation curve of *BiOI* and (b) corresponding first-order dynamics curve.

photocatalytic degradation of RhB dye, benzoquinone (BQ), Methanol and isopropanol (IPA) were added into flower-like BiOI reaction system, which was used as scavengers of superoxide radicals ($^{\bullet}O_2^-$), photo-holes (h^+) and hydroxyl radicals ($^{\bullet}OH$), respectively. As shown in Fig. 9, the photocatalytic degradation rate of RhB reduced significantly after the addition of a trapping agent in the system, which suggested that $^{\bullet}OH$, $^{\bullet}O_2^-$ and h^+ all played a certain role in the photocatalytic degradation process.

8. Analysis of the photocatalytic mechanism

Combined with the above experimental results, the possible photocatalytic degradation mechanism of flower-like BiOI under simulated visible light irradiation is illustrated in Fig. 10. The E_g, E_{CB} and E_{VB} of P-type BiOI semiconductors are 1.93, –0.46 and 1.47 eV, respectively. Under simulated visible light irradiation, photoelectrons are excited simultaneously from VB to CB of BiOI semiconductors, while the holes remain in VB, respectively. Since the E_{CB} of BiOI is more negative than E_0 (–0.28 V vs NHE), electrons in the conduction band can be captured by dissolved oxygen in the water to generate $^{\bullet}O_2^-$. While the holes in the VB of BiOI can react with $^{\bullet}OH$ or H_2O to form hydroxyl radical $^{\bullet}OH$ and $^{\bullet}O_2^-$, which have strong oxidation ability, and h^+ itself is also an oxidant, which can oxidize RhB into CO_2, H_2O and so on at room temperature.

9. Conclusions

BiOI nanopowders with different morphologies (flower-like, microspherical and layered) were successfully fabricated by the co-precipitation method by changing the solvent dosage and pH value. The samples prepared by this method maintain a single-phase tetragonal structure with a small crystallite size and good crystallization. flower-like BiOI exhibit excellent visible light absorption ability, compared with microspherical and layered BiOI, the absorption edge of flower-like BiOI moved to the long-wave direction, with the narrowest bandgap. Microspherical BiOI displays the best photocatalytic activity for RhB degradation under xenon lamp irradiation, and the photocatalytic degradation rate is 92% after 90 min. The active species capture experiments suggested that $^{\bullet}OH$, $^{\bullet}O_2^-$ and h^+ all played a certain role in the photocatalytic degradation process.

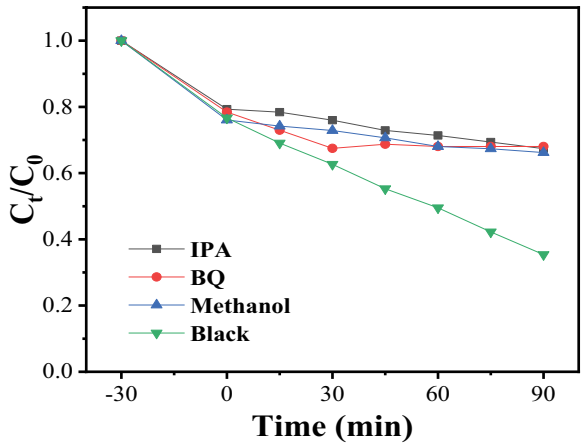

Fig. 9. Active species capture experiment of flower-like *BiOI* photocatalyst.

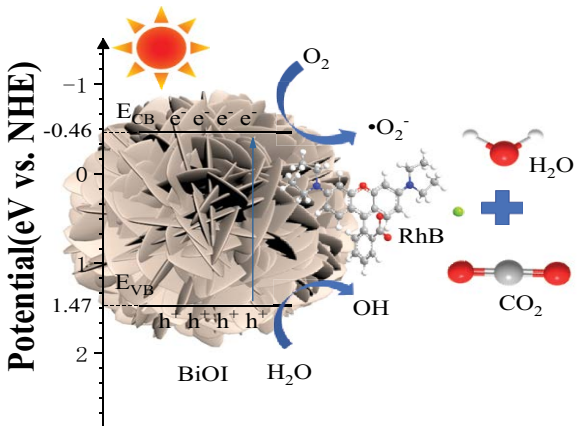

Fig. 10. Possible mechanisms of photocatalytic degradation of *BiOI*.

Acknowledgements

This work was supported by the National Natural Science Foundation of China (51261015), Natural Science Foundation of Gansu Province, China (1308RJZA238) and HongLiu First-Class Disciplines Development Program of Lanzhou University of Technology.

Author contributions

SH and ZW contributed to the content framework of the study. JM and LL gave its suggestions on data analysis. The first draft of the manuscript was written by JZ and all authors provided comments for it. All authors read and approved the final manuscript.

Data availability

All data that support the findings of this study are included within the article.

Declarations

Conflict of interest: There is no conflict of interest to declare.

References

[1] H. Fang, Z. Lin, X. Fu, Spatial variation, water quality, and health risk assessment of trace elements in groundwater in Beijing and Shijiazhuang, North China Plain Environ, Environ. Sci. Pollut. Res., 28 (2021) 57046–57059.
[2] Y. Li, F. Wang, J. Feng, J. Lv, Q. Liu, F. Nan, X. Liu, L. Xu, S. Xie, Spatio-temporal variation and risk assessment of hydrochemical indices in a large diversion project of the Yellow River, northern China, from 2008 to 2017, Environ. Sci. Pollut. Res., 27 (2020) 28438–28448.

[3] Q. Zhang, E. Xu, J. Li, Q. Chen, L. Ma, E. Zeng, H. Shi, A review of microplastics in table salt, drinking water, and air: direct human exposure, Environ. Sci. Technol., 54 (2020) 3740–3751.
[4] N.T. Phong, H.V. Tien, Water resource management and island tourism development: insights from Phu Quoc, Kien Giang, Vietnam, Environ. Dev. Sustainability, 23 (2021) 17835–17856.
[5] D. Ji, C. Xiao, S. An, J. Zhao, J. Hao, K. Chen, Preparation of high-flux PSF/GO loose nanofiltration hollow fiber membranes with dense-loose structure for treating textile wastewater, Chem. Eng. J., 363 (2019) 33–42.
[6] H. Wang, L. Lu, H. Chen, A.M. Mckenna, J. Lu, S. Jin, Y. Zuo, F.L. Rosario-Ortiz, Z. Ren, Molecular transformation of crude oil contaminated soil after bioelectrochemical degradation revealed by FT-ICR mass spectrometry, Environ. Sci. Technol., 54 (2020) 2500–2509.
[7] M. Gmurek, J.F. Gomes, R.C. Martins, R.M. Quinta-Ferreira, Comparison of radical-driven technologies applied for paraben mixture degradation: mechanism, biodegradability, toxicity and cost assessment, Environ. Sci. Pollut. Res., 26 (2019) 37174–37192.
[8] X. Liu, Z. Guo, L. Zhou, J. Yang, H. Cao, M. Xiong, Y. Xie, G. Jia, Hierarchical biomimetic $BiVO_4$ for the treatment of pharmaceutical wastewater in visible-light photocatalytic ozonation, Chemosphere, 222 (2019) 38–45.
[9] M. Figueredo, E.M. Rodriguez, J. Rivas, F.J. Beltran, Kinetic model basis of ozone/light-based advanced oxidation processes: a pseudoempirical approach, Environ. Sci. Water Res. Technol., 6 (2020) 1176–1185.
[10] Z. Li, Z. Zhang, L. Wang, X. Meng, Bismuth chromate (Bi_2CrO_6): a promising semiconductor in photocatalysis, J. Catal., 382 (2020) 40–48.
[11] B. Liu, H. Wu, I.P. Parkin, New insights into the fundamental principle of semiconductor photocatalysis, ACS Omega, 5 (2020) 14847–14856.
[12] M. Arumugam, M.Y. Choi, Recent progress on bismuth oxyiodide (BiOI) photocatalyst for environmental remediation, J. Ind. Eng. Chem., 81 (2020) 237–268.
[13] A. Chatterjee, P. Kar, D. Wulferding, P. Lemmens, S.K. Pal, Flower-like BiOI microspheres decorated with plasmonic gold nanoparticles for dual detoxification of organic and inorganic water pollutants, ACS Appl. Nano Mater., 3 (2020) 2733–2744.
[14] F. Li, L. Cheng, J. Fan, Q. Xiang, Steering the behavior of photogenerated carriers in semiconductor photocatalysts: a new insight and perspective, J. Mater. Chem. A, 9 (2021) 23765–23782.
[15] X. Ye, T. Zhu, Z. Hui, X. Wang, J. Wei, S. Chen, Revealing the transfer mechanisms of photogenerated charge carriers over g-C_3N_4/$ZnIn_2S_4$ composite: a model study for photocatalytic oxidation of aromatic alcohols with visible light, J. Catal., 401 (2021) 149–159.
[16] K.M. Alam, P. Kumar, P. Kar, U.K. Thakur, S. Zeng, K. Cui, K. Shankar, Enhanced charge separation in g-C_3N_4-BiOI heterostructures for visible light driven photoelectrochemical water splitting, Nanoscale Adv., 1 (2019) 1460–1471.
[17] F. Zhang, Y. Shao, M. Shu, C. Li, Y. Zheng, Exceptional photocarriers separation efficiency over Bi_2WO_6/BiOI chemical bonding interface for removal organic pollutant, J. Inorg. Organomet. Polym. Mater., 31 (2021) 3262–3271.
[18] S. Gong, G. Zhu, I.A. Bello, F. Rao, S. Li, J. Gao, S.M. Zubairu, J. Peng, M. Hojamberdiev, Constructing 1D/2D BiOI/$ZnWO_4$ P-N heterojunction photocatalyst with enhanced photocatalytic removal of NO, J. Chem. Technol. Biotechnol., 95 (2020) 1705–1716.
[19] Y. Zhou, P. Yan, J. Jia, S. Zhang, X. Zheng, L. Zhang, B. Zhang, J. Chen, W. Hao, G. Chen, Q. Xu, B. Han, Supercritical CO_2 constructed intralayer $[Bi_2O_2]^{2+}$ structural distortion for enhanced CO_2 electro-reduction, J. Mater. Chem. A, 8 (2020) 13320–13327.
[20] H. Ji, C. Hu, S. Zhang, L. Zhang, X. Yang, $BiO(OH)_3I_{1-x}$ solid solution with rich oxygen vacancies: interlayer guest hydroxyl for improved photocatalytic properties, J. Colloid Interface Sci., 605 (2022) 1–12.
[21] J. Wang, Y. Huang, J. Guo, J. Zhang, X. Wei, F. Ma, Optoelectronic response and interfacial properties of BiOI/BiOX (X=F, Cl, Br) heterostructures based on DFT investigation, J. Solid State Chem., 284 (2020) 121181, doi: 10.1016/j.jssc.2020.121181.
[22] S. Huang, Z. Wei, M. Ding, C. Li, Q. Lu, Photo-electrochemical and photocatalytic properties of hierarchical flower-like BiOI/$CoFe_2O_4$ nanocomposites synthesized by co-precipitation method, Opt. Mater., 111 (2021) 110643, doi: 10.1016/j.optmat.2020.110643.
[23] H. Zhang, M. Li, W. Wang, G. Zhang, Q. Tang, J. Cao, Designing 3D porous BiOI/Ti_3C_2 nanocomposite as a superior coating photocatalyst for photodegradation RhB and photoreduction Cr(VI), Sep. Purif. Technol., 272 (2021) 118911, doi: 10.1016/j.seppur.2021.118911.
[24] P. Zhang, H. Liu, H. Liang, J. Bai, C. Li, Enhanced charge separation of α-Bi_2O_3-BiOI hollow nanotube for photodegradation antibiotic under visible light, Chem. Res. Chin. Univ., 36 (2020) 1227–1233.
[25] L. Chen, L. Shi, J. Wu, Z. Tong, C. Huang, C. Li, B. Ou, C. Peng, L. Tian, J. Tang, N-$SrTiO_3$ nanoparticle/BiOBr nanosheet as 0D/2D heterojunctions for enhanced visible light photocatalytic dye degradation, Mater. Sci. Eng., B, 261 (2020) 114667, doi: 10.1016/j.mseb.2020.114667.
[26] L. Chen, J. Wu, L. Shi, J. Yan, X. Zheng, S. Liao, H. Wang, B. Ou, L. Tian, $Bi_2O_2(OH)NO_3$/BiOCl nanocomposite with enhance photodegradation activity under simulated sunlight irradiation, J. Mater. Sci.: Mater. Electron., 33 (2022) 270–282.
[27] S. Chu, Y. Pan, Y. Wang, H. Zhang, H. Xiao, Z. Zou, Polyimide-based photocatalysts: rational design for energy and environmental applications, J. Mater. Chem. A, 8 (2020) 14441–14462.
[28] S. Subudhi, S.P. Tripathy, K.Parida, Highlights of the characterization techniques on inorganic, organic COF and hybrid MOF photocatalytic semiconductors, Catal. Sci. Technol., 11 (2021) 392–415.
[29] L. Xu, X. Huang, S. Xiong, Z. Wang, B. Peng, Z. Ma, J. Zeng, H. Li, S. Tang, Z. Li, L. Wang, Type-II CeO_2(111)/hBN vdW heterojunction for enhanced photocatalytic hydrogen evolution: a first principles study, Int. J. Hydrogen Energy, 46 (2021) 25060–25069.
[30] H.A. Rafaie, N.A.A.M. Nazam, N.I.T. Ramli, R. Mohamed, M.F. Kasim, Synthesis, characterization and photocatalytic activities of Al-doped ZnO for degradation of methyl orange dye under UV light irradiation, J. Aust. Ceram. Soc., 57 (2021) 479–488.
[31] M. Liu, P. Li, S. Wang, Y. Liu, J. Zhang, L. Chen, J. Wang, Y. Liu, Q. Shen, P. Qu, H. Sun, Hierarchically porous hydrangea-like In_2S_3/In_2O_3 heterostructures for enhanced photocatalytic hydrogen evolution, J. Colloid Interface Sci., 587 (2021) 876–882.
[32] P. Nian, L. Shen, F. Zhang, Y. Zhang, G. Wang, D. Chen, Effect of the solution acidic-basic property on the structure and photocatalytic performance of hydrothermally-synthesized TiO_2, Mater. Lett., 324 (2022) 132787, doi: 10.1016/j.matlet.2022.132787.
[33] S. Munro, M. Åhlén, O. Cheung, A. Sanna, Tuning Na_2ZrO_3 for fast and stable CO_2 adsorption by solid state synthesis, Chem. Eng. J., 388 (2020) 124284, doi: 10.1016/j.cej.2020.124284.
[34] Q. Lu, Z. Wei, C. Li, J. Ma, L. Li, Photocatalytic degradation of methyl orange by noble metal Ag modified semiconductor Zn_2SnO_4, Mater. Sci. Semicond. Process., 138 (2022) 106290, doi: 10.1016/j.mssp.2021.106290.
[35] W. Zhao, Z. Wei, L. Zhang, X. Wu, X. Wang, Cr doped SnS_2 nanoflowers: preparation, characterization and photocatalytic decolorization, Mater. Sci. Semicond. Process., 88 (2018) 173–180.